

Multiplexed image storage by electromagnetically induced transparency in a solidG. Heinze,^{*} N. Rentsch, and T. Halfmann[†]*Institut für Angewandte Physik, Technische Universität Darmstadt, Hochschulstraße 6, 64289 Darmstadt, Germany*

(Received 28 June 2012; published 30 November 2012)

We report on frequency- and angle-multiplexed image storage by electromagnetically induced transparency (EIT) in a $\text{Pr}^{3+}:\text{Y}_2\text{SiO}_5$ crystal. Frequency multiplexing by EIT relies on simultaneous storage of light pulses in atomic coherences, driven in different frequency ensembles of the inhomogeneously broadened solid medium. Angular multiplexing by EIT relies on phase matching of the driving laser beams, which permits simultaneous storage of light pulses propagating under different angles into the crystal. We apply the multiplexing techniques to increase the storage capacity of the EIT-driven optical memory, in particular to implement multiplexed storage of larger two-dimensional amounts of data (images). We demonstrate selective storage and readout of images by frequency-multiplexed EIT and angular-multiplexed EIT, as well as the potential to combine both multiplexing approaches towards further enhanced storage capacities.

DOI: [10.1103/PhysRevA.86.053837](https://doi.org/10.1103/PhysRevA.86.053837)

PACS number(s): 42.50.Gy, 42.30.Va, 32.80.Qk, 42.70.Ln

I. INTRODUCTION

Coherent interactions between light and quantum systems offer promising possibilities to develop novel mechanisms for optical data storage, in particular when keeping an eye on potential applications beyond classical information science. Adiabatic passage processes are a specific class of coherent light-matter interactions, which combine efficiency with pronounced robustness [1]. As a prominent example, we note the phenomenon of electromagnetically induced transparency (EIT) [2], which already evolved into a well-established tool for adiabatic data storage. EIT permits significant control of optical properties in a quantum system, for example, absorption and dispersion. Thus, EIT makes it possible to dramatically slow down the speed of a light pulse in a quantum system, or even to stop the pulse and transfer it into an atomic coherence in the medium. If we consider the light pulse as a carrier of information, the preparation of an atomic coherence by EIT can be understood as the “write” process of an optical data bit.

Light storage via EIT is typically implemented in a three-level system in Λ -type configuration (see Fig. 1, left-hand side). A weak probe pulse drives the transition between the ground state $|1\rangle$ and the excited state $|3\rangle$. A strong control pulse couples the metastable state $|2\rangle$ with the excited state $|3\rangle$. The Rabi frequencies are $\Omega_p(t) = \mu_{13}E_p(t)/\hbar$ and $\Omega_c(t) = \mu_{23}E_c(t)/\hbar$, with transition dipole moments μ_{ij} and electric fields $E(t)$. If the control pulse is sufficiently strong and we switch off the temporally overlapping pulses adiabatically (i.e., sufficiently slow), the probe pulse is transformed into an atomic coherence ρ_{12} between the two lower states $|1\rangle$ and $|2\rangle$. This corresponds to writing an optical data bit into the quantized memory. After some storage time we apply the control field again to beat with the coherence, which generates a copy of the probe pulse (i.e., a signal pulse propagating at the same direction and with the same frequency and phase as the initial probe pulse). Thus, the initial probe

pulse is restored into a signal pulse. This corresponds to reading the quantized memory into an optical data bit. The ratio of the signal pulse energy and the initial probe pulse energy serves as a simple measure for the storage efficiency η .

There are already many experiments on light storage by EIT (see, e.g., [3] and references therein). However, the vast majority of the implementations deals with pulses of uniform spatial profile, which do not carry image information. As a rather straightforward extension, light storage by EIT is also possible for complex spatial profiles, that is, images imprinted on the probe beam. This increases the storage capacity of EIT by many orders of magnitude. First experiments dealing with image storage by EIT were conducted in atomic gases [4,5]. However, atomic diffusion in gases limits the storage time of images to the range of some 10 μs . Diffusion is no problem in solid media, for example, in rare-earth-ion-doped crystals. The latter media combine the advantages of gases (i.e., small homogeneous linewidths and long decoherence times) with the advantages of solids (i.e., large optical storage densities and scalability). Hence, in a previous publication we reported about successful implementation of image storage by EIT in a doped crystal. By additional application of simple rephasing techniques, the storage times in the solid extended into the millisecond range, that is, two orders of magnitude beyond the maximal storage times in atomic gases [6].

With regard to future applications, it is highly desirable to further increase the storage capacity of EIT-driven quantum systems. Although such devices are mostly considered as memories of low bandwidth, there are ways to increase the storage bandwidth. To achieve the goal of high storage capacity, we combine EIT with multiplexing methods from holographic data storage. The latter exhibit probably the most powerful conventional approaches for high-capacity optical memories [7]. However, in classical holography it is not possible to store the temporal shape of a pulse (or sequences of pulses) [8], that is, information spread in the time domain. To overcome this drawback, time-domain frequency-selective optical data storage techniques were proposed [9]. The first demonstration of this approach was implemented in $\text{Eu}^{3+}:\text{Y}_2\text{O}_3$ [10]. Afterwards, the work in Refs. [11–13] showed the application of time-domain optical memories

^{*}georg.heinze@physik.tu-darmstadt.de[†]<http://www.iap.tu-darmstadt.de/nlq>

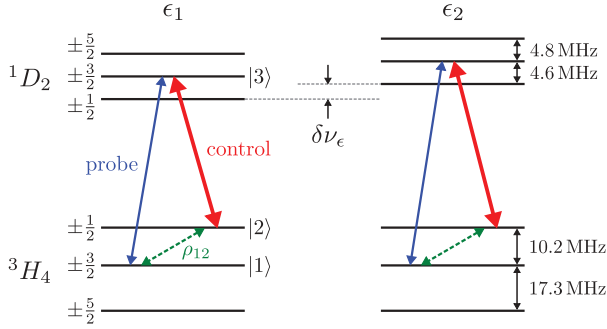


FIG. 1. (Color online) Coupling scheme in $\text{Pr}^{3+}:\text{Y}_2\text{SiO}_5$ for two frequency ensembles ϵ_1, ϵ_2 of dopant ions with a frequency separation of $\delta\nu_\epsilon$.

(TDOM) to store a large number of pulses or even images by different multiplexing techniques. However, all of these classical techniques are not suitable for quantum state storage, as they apply dissipative or amplifying elements [14,15]. Hence, multiplexed storage of light pulses based on coherent light-matter processes from the background of quantum optics (e.g., EIT) gained considerable attention in recent years [16–19].

As we demonstrate in our work, the combination of light storage by EIT with frequency- and angle-resolved multiplexing permits simultaneous storage of images in the solid memory. Conceptually, EIT-driven frequency multiplexing relies on the separate addressability of different frequency classes of dopant ions in the solid. This is due to a large inhomogeneous broadening of the relevant optical transition. EIT-driven angular multiplexing relies on the application of several control and probe beams with different angles in between. Due to phase matching, the information on different directions of the driving beams is also encoded in the medium and can be read out selectively into different signal beams. Both multiplexing approaches can be combined to increase the storage capacity even further. In the following we present experiments to simultaneously store two images either by frequency-multiplexed EIT or angle-multiplexed EIT in a rare-earth-ion-doped solid. Moreover, we also demonstrate a combination of both approaches to store four light pulses simultaneously in the solid medium.

We note that Tu *et al.* previously reported on some first experiments of angular-multiplexed EIT in a doped crystal to store light pulses (without image information) [17]. We go well beyond related previous work by implementation both of frequency multiplexing and angular multiplexing, combination of the two approaches, application to multiplexed image storage, as well as prolongation of storage times by two orders of magnitude.

II. EXPERIMENTAL SETUP

Figure 2 shows the small part of the experimental setup, which is relevant for the present work. The experiments are implemented in a $\text{Pr}^{3+}:\text{Y}_2\text{SiO}_5$ crystal (hereafter termed Pr:YSO), with a length of 3 mm and a dopant concentration of 0.02%. The crystal is placed inside a liquid helium cryostat to keep the temperature below 4 K and reduce interactions with phonons. A single-longitudinal-mode dye laser (Sirah

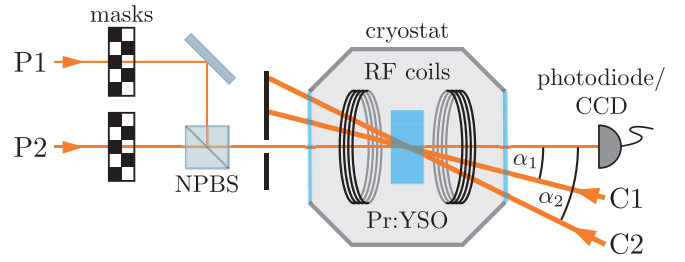


FIG. 2. (Color online) Experimental setup. The two control beamlines C1 and C2 pass the weak probe beamlines P1 and P2 under angles of $\alpha_1 = 1.5^\circ$ and $\alpha_2 = 2.7^\circ$ in air. In the experiments on frequency multiplexing we use the probe beamlines P1 and P2, as well as control beamline C1. In the experiments on angular multiplexing we use all four beamlines P1, P2, C1, and C2.

Matisse DX) provides continuous radiation at 605.98 nm to drive the optical transition between the electronic ground state 3H_4 and the excited state 1D_2 in Pr:YSO (see also Fig. 1). The radiation is split up into four beamlines with full independent control of the temporal frequency and intensity profiles by acousto-optic modulators. All beams are linearly polarized along the D_2 axis of the crystal. The two beamlines labeled P1 and P2 in Fig. 2 provide rather weak probe pulses with maximal power of $P_{P1,P2} \approx 6$ mW. The probe beams pass binary masks to imprint image information on their spatial profiles. A nonpolarizing beamsplitter cube (NPBS) superimposes the probe beams, which then propagate collinearly through the crystal. The diameters of the probe beams in the crystal are $\varnothing_{P1} = 150 \mu\text{m}$ and $\varnothing_{P2} = 215 \mu\text{m}$ (full width at half maximum of intensity). The two beamlines labeled C1 and C2 in Fig. 2 provide intense control beams with maximal powers of $P_C \approx 60$ mW. The diameters of the control beams (with Gaussian spatial profile) in the interaction region are $\varnothing_{C1} = 340 \mu\text{m}$ and $\varnothing_{C2} = 290 \mu\text{m}$. Hence, the probe beams interact only with ions which are entirely prepared by the control beams. Two radio-frequency (RF) coils close to the crystal inside the cryostat permit rephasing of the laser-driven atomic coherences and prolongation of storage times. To create the RF pulses we use a RF switch and cut out pulses of a continuous sine wave provided by an arbitrary waveform generator. Retrieved signal pulses are detected by a photodiode (New Focus, Model 2051) or alternatively retrieved images by a CCD camera (Prosilica GC1290).

III. FREQUENCY MULTIPLEXING

Figure 1 shows the coupling scheme of Pr^{3+} ions in the doped crystal. The electronic ground state 3H_4 and the optically excited state 1D_2 consist of three doubly degenerate hyperfine states. These levels are labeled according to their magnetic quantum numbers m_I and exhibit frequency splittings in the range of 10 MHz. The assignment of hyperfine states to the three-level Λ -type coupling scheme in EIT is as follows: State |1> corresponds to $|^3H_4, m_I = \pm \frac{3}{2}\rangle$, state |2> corresponds to $|^3H_4, m_I = \pm \frac{1}{2}\rangle$, and state |3> corresponds to $|^1D_2, m_I = \pm \frac{3}{2}\rangle$. The radiative population lifetime in the hyperfine levels of the excited state 1D_2 is $T_1^* = 164 \mu\text{s}$ and the decoherence time is $T_2^* = 111 \mu\text{s}$. The radiative population lifetime in the hyperfine levels of the ground state 3H_4 is $T_1 \sim 100$ s [20] and

the decoherence time is $T_2 = 500 \mu\text{s}$ [21]. Due to spatially varying electric fields in the crystal, the frequency of the transition between states 3H_4 and 1D_2 changes for different ensembles of ions. Thus, we get an inhomogeneous broadening of the optical transition in the range of several GHz, while the homogeneous linewidth is 3 kHz only [22]. This permits selective addressing of different frequency ensembles in the inhomogeneous bandwidth by appropriate optical preparation and appropriate choice of the probe and control frequencies. As an example, Fig. 1 depicts two frequency ensembles ϵ_1 and ϵ_2 in the inhomogeneously broadened manifold.

We note that the storage times in the doped solid are limited by decoherence (i.e., stochastic fluctuations of the phases in atomic coherences) and dephasing (i.e., smooth phase drifts of atomic coherences due to inhomogeneous broadening). The decoherence time of the hyperfine levels in state 3H_4 is $500 \mu\text{s}$. The dephasing time is in the range of $10 \mu\text{s}$ only [23]. This limits the maximal storage times in atomic coherences significantly. While it is hard to cope with stochastic decoherence, it is rather simple to compensate smooth dephasing processes by rephasing strategies. Instead of optical [21,24] or electric [25,26] rephasing, we use RF π pulses to overcome dephasing in our experiments. Radio-frequency pulses are experimentally easy to implement (consider, e.g., the issue of phase stability in the optical regime) and directly address the atomic coherence on a magnetic single-photon transition. In our case, the frequency of the rephasing pulses is $\nu_{\text{RF}} = 10.2 \text{ MHz}$, that is, resonant with the RF transition between states $|1\rangle$ and $|2\rangle$. The RF π pulses drive an inversion of the phase evolution of individual atomic coherences in both ensembles ϵ_1 and ϵ_2 (see Fig. 1) to restore the total initial coherence. This enables storage times towards the regime of the decoherence time (i.e., $500 \mu\text{s}$) and provides a comfortable time frame for our measurements. We note that we apply two rephasing RF π pulses between the optical write and read process. Hence, for readout the ions are again in the ground state and do not contribute to noise generated by amplified spontaneous emission. However, between the RF pulses the ions are in the excited state, which may lead to gain. This is a serious problem in optical photon echo experiments, that is, when the coherence is created between a ground state and an optically excited state. The first echo (between the RF pulses) would be amplified and carry away parts of the stored information as it leaves the crystal. Hence, strategies to silence the first echo based on Stark effects [27] or spatial phase mismatch [28] were developed. However, in EIT experiments this is not an issue, as the coherence is created between two metastable ground states. The latter do not lead to stimulated emission on an optical transition. The optical signal field (respectively the second echo) evolves only in the very last step, that is, when the intense control field beats with the stored ground-state coherence. This avoids noise due to stimulated emission during the storage time. For details on rephasing in EIT-driven light storage we refer the reader to our previous work on related subjects [6].

To selectively prepare frequency ensembles of dopant ions for the light-storage experiments we apply a pulse sequence from beamline C1 [see Fig. 3(b)]. The sequence starts with a first step to prepare a “spectral pit” (i.e., a broader region of vanishing absorption) close to the maximum of

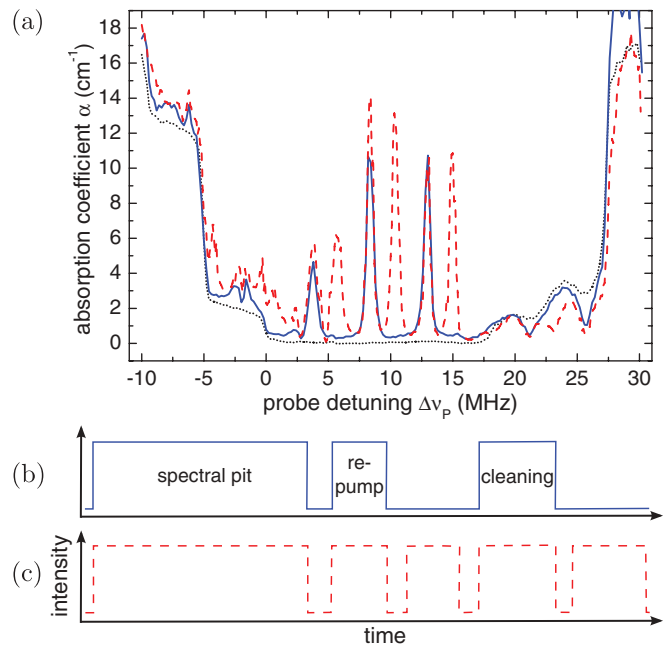


FIG. 3. (Color online) Preparation of two frequency ensembles in the doped solid by optical pumping. (a) Experimentally recorded absorption spectra. Black dotted line, spectral pit after first preparation step with a frequency chirped pulse; blue solid line, spectrum after additional application of a single repump pulse and a single cleaning pulse; red dashed line, spectrum after application of two repump and cleaning pulses with frequency spacings of $\delta\nu_\epsilon = 2 \text{ MHz}$. (b) Schematic pulse sequence for preparation of a single frequency ensemble (blue solid line). (c) Schematic pulse sequence for preparation of two frequency ensembles (red dashed line).

the inhomogeneously broadened optical transition by optical pumping with frequency chirped pulses [20,23]. The black dotted line in Fig. 3(a) shows the experimentally determined absorption spectrum of the spectral pit, generated after the first step of the preparation sequence. In the following we describe all laser frequencies and detunings relative to the left edge of the spectral pit. In a second step we add a short pulse at a relative frequency of $\Delta\nu_{\text{rep.}} = 25.7 \text{ MHz}$ to repump population into the spectral pit, that is, into states $|1\rangle$ and $|2\rangle$. A third pulse with a relative frequency of $\Delta\nu_{\text{clean}} = 2.8 \text{ MHz}$ “cleans” state $|2\rangle$ and transfers the entire population into state $|1\rangle$. This sequence generates a set of three major absorption lines in the spectrum [see blue solid line in Fig. 3(a)]. These lines correspond to the possible transitions from state $|1\rangle$ to the hyperfine levels of excited state 1D_2 . To prepare two frequency ensembles in parallel, we extend the preparation sequence by a second repump and a second cleaning pulse at slightly different frequencies with regard to the first repump and cleaning pulse [see Fig. 3(c)]. The red dashed line in Fig. 3(a) shows the absorption spectrum, generated by this simple extended sequence. The spectrum contains now twice a triplet of absorption lines, which correspond to transitions from different frequency ensembles, prepared in state $|1\rangle$. We note that we choose the frequency separation $\delta\nu_\epsilon$ of the repump and cleaning pulses sufficiently large compared to the Rabi frequency of the control pulses. This enables selective

addressing of two ensembles by the control pulses during the light storage experiments.

After preparation of the two frequency ensembles ϵ_1 and ϵ_2 we apply now an extended version of EIT to simultaneously store two light pulses (or images, respectively) in the same spatial region of the Pr:YSO crystal.

For frequency-multiplexed light storage we use the probe beamlines P1 and P2 to provide probe pulses at different frequencies, as well as beamline C1 to provide sequences of control pulses at different frequencies (compare Fig. 2). On the spatial profiles of the two probe pulses we imprint different images (horizontal lines on beamline P1 and vertical lines on beamline P2). The top part of Fig. 4 shows the pulse sequences in the frequency multiplexing experiment. We record these pulse sequences (involving also the retrieved signal pulses) on a photodiode. In Fig. 4 and similar following figures we denote probe pulses by “p”, control write and read pulses by “w” and “r”, respectively, and retrieved signal pulses by “s”. To drive simultaneous data storage and retrieval in two frequency ensembles, we apply two pairs of probe and control pulses, that is, a first pulse pair (p1,w1) and a second pulse pair (p2,w2). The laser frequencies of each pair are

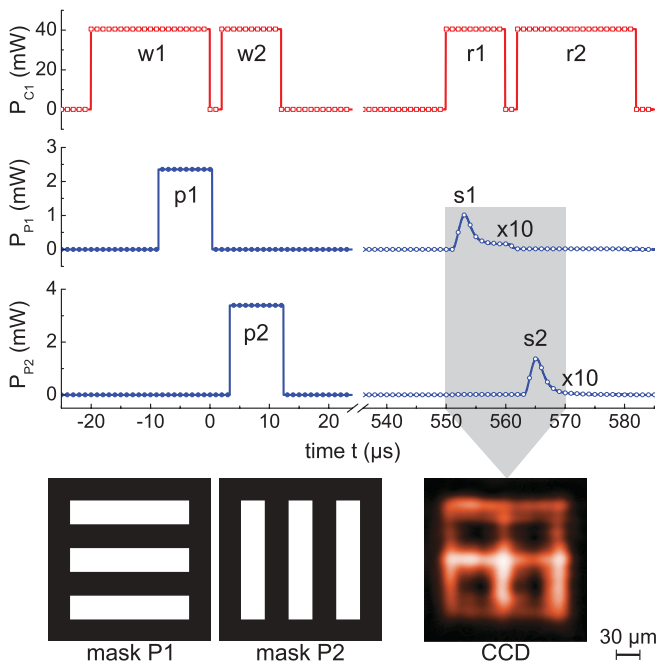


FIG. 4. (Color online) (Top) Pulse sequences (experimental data) for frequency-multiplexed light storage. Laser powers of control write and read pulses (red open squares), probe pulses (blue solid circles), and retrieved signal pulses (blue open circles). We denote single probe pulses by “p”, control write and read pulses by “w” and “r”, and retrieved signal pulses by “s”. The peak Rabi frequencies of the probe and control pulses are $\Omega_{p1} = 2\pi \times 264$ kHz, $\Omega_{p2} = 2\pi \times 221$ kHz and $\Omega_{C1} = 2\pi \times 392$ kHz. The frequency detunings of the probe and control pulses are $\Delta\nu_{p1} = 13$ MHz, $\Delta\nu_{p2} = 15$ MHz, $\Delta\nu_{w1,r1} = 2.8$ MHz, $\Delta\nu_{w2,r2} = 4.8$ MHz. In order not to overload the figure, we do not depict the RF rephasing pulses between the optical write and read processes. (Bottom) Image masks on the probe beams P1 and P2 (left). Sum of the spatial profiles of the signal pulses s1 and s2 after a storage time of $\Delta t = 550 \mu\text{s}$ (right). The gray shaded area illustrates the exposure time of the CCD camera.

tuned to the probe and control transition in one of the two ensembles (compare Fig. 1). The control write pulse w1 and probe pulse p1 interact to store the first image (horizontal lines) in atomic coherences in ensemble ϵ_1 . Then the control write pulse w2 and probe pulse p2 interact to store the second image (vertical lines) in atomic coherences in ensemble ϵ_2 . After a storage time of $\Delta t = 550 \mu\text{s}$ we apply a control read pulse r1 to retrieve a signal pulse s1 from the atomic coherence in the first frequency ensemble ϵ_1 . Afterwards, we apply a control read pulse r2 to retrieve a signal pulse s2 from the atomic coherence in the second frequency ensemble ϵ_2 . For a first demonstration of frequency-multiplexed image storage, we monitor the spatial profiles of the signal beams on a CCD camera with an exposure time of $20 \mu\text{s}$, that is, covering both signal pulses (see Fig. 4, bottom). The sum of the signal beam profiles reveals the image information (i.e., horizontal and vertical lines), which was initially encoded on the probe beams and stored simultaneously by frequency multiplexed EIT in the Pr:YSO crystal. We optimized this and all following images shown in this paper by subtracting a background image (taken without probe beams) and averaging over 400 frames. We note that the retrieval efficiency η (i.e., the ratio of the signal pulse energy with regard to the initial probe pulse energy) is rather low in the experiment. We get efficiencies of $\eta_1 = 1.63\%$ and $\eta_2 = 1.28\%$ for the two signal pulses s1 and s2. The low efficiencies are mainly attributed to off-resonant interactions between the applied control pulses and the prepared coherences of both ensembles ϵ_1 and ϵ_2 . Moreover, also the overall low optical depth of the crystal and an imperfect RF rephasing contribute to the reduced storage efficiency. However, this does not matter for the demonstration of EIT multiplexing.

The above experiment already demonstrates frequency multiplexed storage of two images in atomic coherences. However, this does not yet prove the possibility to *selectively* write and read information in the two ensembles without cross-talk in between. Thus, we performed additional measurements: (a) Selectively writing a single probe pulse p1 or p2 with the corresponding control write pulse w1 or w2, but checking readout by both control read pulses r1 and r2. (b) Writing both probe pulses p1 and p2 with the corresponding control write pulses w1 and w2, but checking readout by a single control read pulse r1 or r2.

To investigate selective writing, we apply the same pulse sequence as depicted in the upper part of Fig. 4, but with only one probe pulse p1 (or p2). Upon readout with both control pulses r1 and r2 we should get now an image only in channel s1 (or s2), but no image in the other beam. Figure 5(a) shows the results of this experiment. The matrix on the left shows the masks for the input probe beams. The matrix on the right shows the retrieved images on the signal beams. As the data clearly indicate, in both channels the image information is correctly stored and retrieved without cross-talk between the atomic coherences in the two ensembles. If we write selectively only in one channel p, we get only an image in the corresponding signal channel s, but no image in the other signal channel.

To investigate selective readout, we applied a pulse sequence as depicted in Fig. 4, but with only one control readout pulse r1 (or r2). Thus, we store now simultaneously two images with probe pulses p1 and p2 in the medium, but

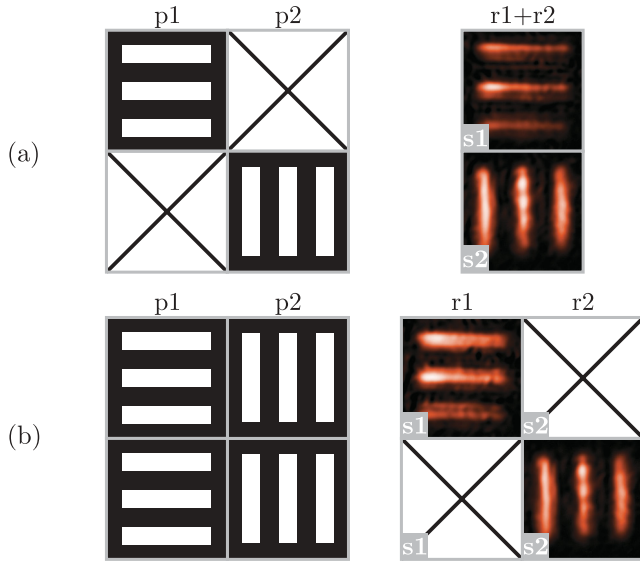


FIG. 5. (Color online) Image storage by frequency multiplexed EIT. The matrices on the left show the input images (i.e., masks on the probe beams). The matrices on the right show the corresponding retrieved images (i.e., spatial profiles of the signal beams). We consider the cases (a) selective writing and simultaneous readout and (b) simultaneous writing and selective readout. As an example on how to read the first line of the graphics, we consider the first line of the matrices in case (b): We simultaneously write two different images with p1 and p2. We readout with r1, while r2 is switched off. On the signal beam s1 we correctly retrieve the image from p1 without cross-talk from the other image.

select only one of them by the readout process. Figure 5(b) shows the results of the experiment. The matrix on the left shows the masks for the input probe beams. The matrix on the right shows the retrieved images on the signal beams. Also upon selective readout the image information in both channels is correctly stored and retrieved without cross-talk between the ensembles. If we read selectively only one channel s, we get the image from the corresponding probe channel p, without perturbation from the other probe channel.

IV. ANGULAR MULTIPLEXING

The basic concept of angular multiplexing is as follows. EIT-driven atomic coherences contain information on the wave vectors of the interacting probe and control write pulses (or the angle between the beams, respectively). This can be easily understood if we consider light storage and retrieval by EIT as a four-wave mixing process of the probe pulse, the control write pulse, and the control read pulse to generate the signal pulse. If the wave vectors of probe, control write, and read pulses are \vec{k}_p , \vec{k}_w , \vec{k}_r , respectively, we get the wave vector of the signal pulse according to $\vec{k}_s = \vec{k}_p - \vec{k}_w + \vec{k}_r$. Efficient readout of atomic coherences requires a phase-matched control read pulse to reduce the phase mismatch $\Delta\vec{k} = \vec{k}_p - \vec{k}_w + \vec{k}_r - \vec{k}_s$ to zero. Thus, to obtain a signal pulse in the direction of the initial probe pulse, we require a control read pulse in the same direction as the previous control write pulse.

Angular multiplexing by EIT relies on simultaneous preparation of atomic coherences in the same interaction volume, driven by pairs of probe and control pulses propagating at different directions. To retrieve a certain probe pulse, we choose the direction of the control read pulse to match with the direction of the previous control write pulse. We note that in angular multiplexing all probe beams operate at the same frequency $\Delta\nu_{p1,p2} = 13$ MHz, and also all control beams exhibit the same frequency $\Delta\nu_{c1,c2} = 2.8$ MHz. We require only a single frequency ensemble of ions in Pr:YSO for angular multiplexing. Thus, preparation of the doped crystal requires an optical pumping sequence involving a single repump and a single cleaning pulse only [see Fig. 3(b)].

For angular multiplexed light storage we use both probe beamlines P1 and P2, as well as both control beamlines C1 and C2 (compare Fig. 2). On the spatial profiles of the two probe pulses we imprint different images (horizontal lines on beamline P1 and vertical lines on beamline P2). To demonstrate angular multiplexed image storage we apply now two pairs (p1,w1) and (p2,w2) of probe and control pulses. The control pulses w1 and w2 interact with the two collinear propagating probe pulses p1 and p2 under slightly different angles α_1 and α_2 . The top part of Fig. 6 shows the pulse sequences in the angular multiplexing experiment, as we monitored it on a photodiode. First we apply a probe

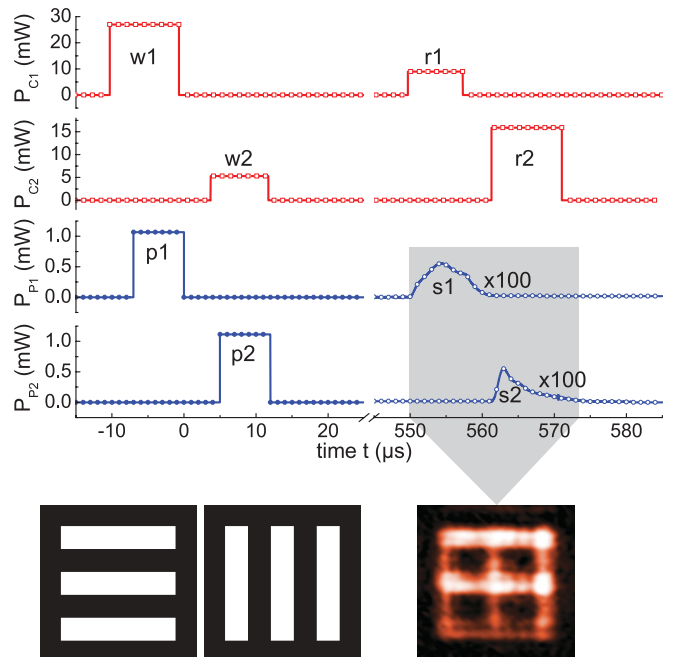


FIG. 6. (Color online) (Top) Pulse sequences (experimental data) for angle multiplexed light storage. Laser powers of control write and read pulses (red open squares), probe pulses (blue solid circles), and retrieved signal pulses (blue open circles). The peak Rabi frequencies of the probe and control pulses are $\Omega_{p1} = 2\pi \times 178$ kHz, $\Omega_{p2} = 2\pi \times 127$ kHz, $\Omega_{c1} = 2\pi \times 320$ kHz, and $\Omega_{c2} = 2\pi \times 288$ kHz. The frequency detunings of the probe and control pulses are $\Delta\nu_{p1,p2} = 13$ MHz and $\Delta\nu_{c1,c2} = 2.8$ MHz. Image masks on the probe beams P1 and P2 (left). Sum of the spatial profiles of the signal pulses s1 and s2 after a storage time of $\Delta t = 550 \mu s$ (right). The gray shaded area illustrates the exposure time of the CCD camera.

pulse p1 with the control write pulse w1 to store the image imprinted on beam P1. Afterwards we apply a probe pulse p2 with the control write pulse w2 to store the image imprinted on beam P2.

After application of RF-rephasing pulses (compare previous section) we introduce two control read pulses r1 and r2 at a storage time of $\Delta t = 550 \mu\text{s}$. The control read pulses propagate in the same direction as the corresponding control write pulses. Thus, we retrieve signal pulses s1 and s2 in the direction of the initial probe pulses. We monitor the spatial profiles of the signal beams on a CCD camera with an exposure time of $23 \mu\text{s}$, that is, covering both signal pulses (see Fig. 6, bottom). The sum of the signal beam profiles reveals the image information (i.e., horizontal and vertical lines), which was initially encoded on the probe beams and stored simultaneously by angular multiplexed EIT in the Pr:YSO crystal.

We note that the retrieval efficiencies $\eta_1 = 0.47\%$ and $\eta_2 = 0.26\%$ are smaller compared to the case of frequency multiplexing (see above). This is due to the fact that in angular multiplexing we use only a single frequency ensemble of ions. Thus, we would expect a drop in efficiency by 50% compared to frequency multiplexing, because now only half of the ions contribute. However, there is also a further reduction due to not fully perfect angular selectivity of the write and read processes (i.e., slightly phase-mismatched readout), as well as erasure of the atomic coherence by the “wrong” control beam [17]. To reduce the latter perturbation, we chose rather weak control pulse powers (in particular for w2 and r1). Thus, unwanted readout is minimized (compare also Fig. 6). However, the reduced control power also reduces the EIT bandwidth. This leads to a larger incoherent absorption of components in the spectrum of the probe pulse, which reduces the storage efficiency. Thus, we expect the efficiency of angular multiplexing in EIT-driven light storage typically to be substantially lower compared to frequency multiplexing.

To demonstrate now the capability of angular multiplexing for *selective* write and read processes, we performed additional measurements: (a) selectively writing a single probe pulse p1 or p2 with the corresponding control write pulse w1 or w2, but checking readout by both control read pulses r1 and r2; (b) writing both probe pulses p1 and p2 with the corresponding control write pulses w1 and w2, but checking selective readout by a single control read pulse r1 or r2.

To investigate selective writing, we applied the same pulse sequence as depicted in the upper part of Fig. 6, but with only one probe pulse p1 (or p2). Figure 7(a) shows the results of this experiment. The matrix on the left shows the masks for the input probe beams. The matrix on the right shows the retrieved images on the signal beams. In both channels the image information is correctly stored and retrieved without perturbation by the other phase-mismatched control read beam. If we write selectively only in one channel p, we get only an image in the corresponding signal channel s, but no image in the other signal channel.

To investigate selective readout, we applied a pulse sequence as depicted in Fig. 6, but with only one control readout pulse r1 (or r2). Figure 7(b) shows the results of the experiment. The matrix on the left shows the masks for the input probe beams. The matrix on the right shows the retrieved images on the signal beams. The image information in both

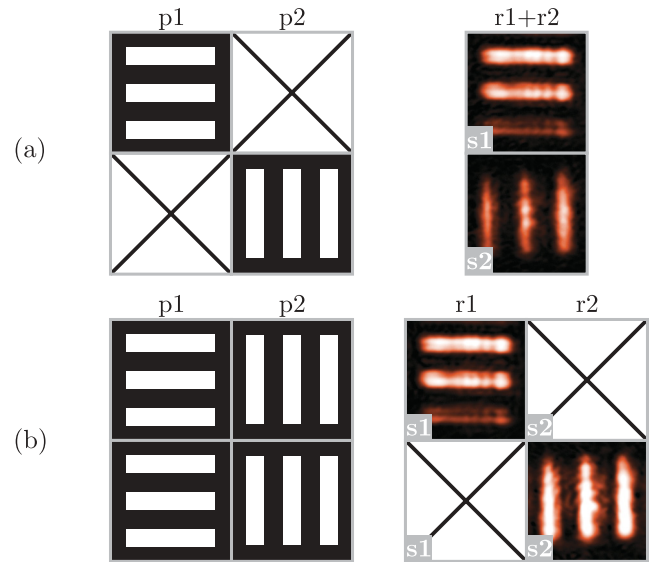


FIG. 7. (Color online) Image storage by angular multiplexed EIT. The matrices on the left show the input images (i.e., masks on the probe beams). The matrices on the right show the corresponding retrieved images (i.e., spatial profiles of the signal beams). We consider the cases (a) selective writing and simultaneous readout and (b) simultaneous writing and selective readout. For an example on how to read the graphics, see caption of Fig. 5.

channels is correctly stored and retrieved without cross-talk between atomic coherences, prepared by control write beams in different directions. If we read selectively only in one channel s, we get the image from the corresponding probe channel p, without perturbation from the other probe channel.

V. COMBINED FREQUENCY-ANGULAR MULTIPLEXING

In the previous sections we demonstrated pure frequency multiplexing or pure angular multiplexing for light storage. It is a straightforward extension to combine these two multiplexing strategies to further increase the storage capacity in the EIT-driven medium. The simple idea is to drive angular multiplexing in several frequency ensembles (rather than in one frequency ensemble only, as presented in the last section). In the following we present a proof-of-principle experiment for combined frequency and angular multiplexing. As the storage efficiencies in our setup were rather low and further decrease by combination of multiplexing channels, we investigated storage of simple light pulses (i.e., without imprinted image information).

The preparation sequence in combined frequency-angular multiplexing is analogous to the case of frequency multiplexing [see Fig. 3(c)]. The pulse sequences for the subsequent light storage experiment are monitored on a photodiode and shown in Fig. 8. From beamline C1 we apply two control write pulses w1 and w2 at slightly different frequencies to interact with two probe pulses p1 and p2 at corresponding frequencies. This stores the probe pulses p1 and p2 in atomic coherences, prepared in two frequency ensembles. Afterwards we copy the pulse sequence to beamline C2 and generate two control write pulses w3 and w4 (at the same frequencies as the pulses w1 or w2, respectively) to store two additional probe pulses p3 and p4

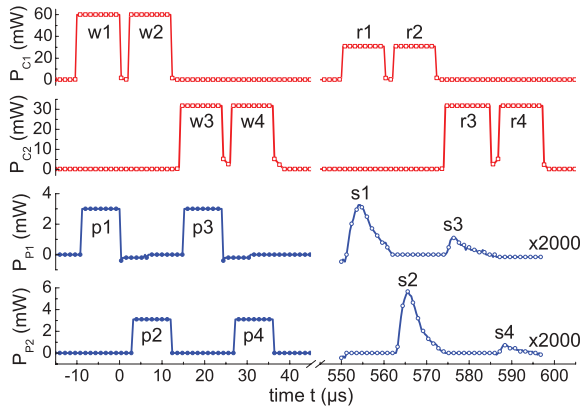


FIG. 8. (Color online) Pulse sequences (experimental data) for combined frequency-angle multiplexed light storage. Laser powers of control write and read pulses (red open squares), probe pulses (blue solid circles), and retrieved signal pulses (blue open circles). The peak Rabi frequencies of the probe and control pulses are $\Omega_{p1,p3} = 2\pi \times 298$ kHz, $\Omega_{p2,p4} = 2\pi \times 212$ kHz, $\Omega_{C1} = 2\pi \times 478$ kHz, and $\Omega_{C2} = 2\pi \times 407$ kHz.

(at the same frequencies as the pulses p1 or p2, respectively) in the two frequency ensembles. As the control beamlines intersect the probe beamlines under different angles, the atomic coherences corresponding to p1 and p2 contain different angle information compared to the coherences corresponding to p3 and p4. Thus, we split the two frequency multiplexed channels in doublets of two angular multiplexed channels each and get a total of four information channels.

For selective readout after rephasing RF pulses and a storage time of $\Delta t = 550$ μ s, we apply control read pulses r1 and r2 from beamline C1 and frequencies corresponding to the control write pulses w1 and w2. As the traces in Fig. 8 clearly show, we retrieve signal pulses s1 and s2. Similarly, when applying control read pulses r3 and r4 from beamline C2 and frequencies corresponding to the control write pulses w3 and w4, we retrieve signal pulses s3 and s4. As expected, the storage efficiencies $\eta_1 = 0.039\%$, $\eta_2 = 0.051\%$, $\eta_3 = 0.013\%$, and $\eta_4 = 0.008\%$ in the combined frequency-angular multiplexing are far smaller compared to pure frequency or angular multiplexing. This is due to the fact that each generated coherence suffers now from residual, perturbing interactions with all subsequent control pulses, for example, phase-mismatched control read pulses. We also note that the signal pulses s1 and s2 are more intense compared to the signal pulses s3 and s4. We attribute this to a better overlap of the probe beamlines P1 and P2 with beamline C1. Due to the smaller angle to beamline C1, the ratio of probe/control laser intensities varies less along the crystal. This permits a more efficient adiabatic conversion of probe pulses p1 and p2 into

atomic coherences. Nevertheless, Fig. 8 clearly demonstrates the potential to combine frequency and angular multiplexing for selective storage and retrieval of light pulses.

VI. CONCLUSION

We presented experimental investigations on light and image storage by EIT, combined with frequency and angular multiplexing approaches to enhance the storage capacity in a $\text{Pr}^{3+}:\text{Y}_2\text{SiO}_5$ crystal. By interaction with a control pulse, EIT permits conversion of a probe pulse into an atomic coherence (and back again), driven between long-lived hyperfine levels in the doped solid. Frequency multiplexing in light storage is based on simultaneous preparation of several frequency ensembles in the inhomogeneous bandwidth of the doped crystal. Appropriate choice of laser frequencies permits selective light storage in different frequency ensembles. Angular multiplexing relies on the fact that atomic coherences also contain information on the angle between the driving probe and control pulses. Due to phase matching conditions, retrieval of light pulses from an atomic coherence is possible only in a certain direction, determined by the wave vectors of the control and probe pulses. This enables selective writing and reading of data by variation of the angle between the driving pulses.

We experimentally demonstrated and investigated the combination of light storage with frequency and angular multiplexing to simultaneously store and selectively read out light pulses and images by EIT in $\text{Pr}^{3+}:\text{Y}_2\text{SiO}_5$. In frequency multiplexing, appropriate choice of probe and control laser frequencies enabled simultaneous or selective writing and reading of two light pulses or images by EIT. In angular multiplexing, appropriate choice of the propagation direction of control pulses also enabled simultaneous or selective writing and reading of two light pulses or images by EIT. Additional RF rephasing pulses permitted prolongation of image storage times towards the regime of the decoherence time in the medium (i.e., 500 μ s). Moreover, we also demonstrated combined frequency-angular multiplexing to store and retrieve four light pulses simultaneously in the doped solid. The investigations shall serve as a step forward towards realistic implementations of larger scale data storage by EIT.

ACKNOWLEDGMENTS

The authors thank D. Schraft and S. Mieth for experimental support and most valuable discussions. The research leading to these results has received funding from Deutsche Forschungsgemeinschaft, the Volkswagen foundation, and the People Programme (Marie Curie Actions) of the European Union's Seventh Framework Programme FP7/2007-2013/ under REA Grant Agreement No. 287252.

- [1] N. V. Vitanov, T. Halfmann, B. W. Shore, and K. Bergmann, *Annu. Rev. Phys. Chem.* **52**, 763 (2001).
 [2] M. Fleischhauer, A. Imamoglu, and J. Marangos, *Rev. Mod. Phys.* **77**, 633 (2005).

- [3] J. P. Marangos and T. Halfmann, in *Handbook of Optics*, Vol. 4, edited by M. Bass, 3rd ed. (McGraw-Hill, Columbus, OH, 2009), Chap. 14, pp. 14.1–14.44.

- [4] M. Shuker, O. Firstenberg, R. Pugatch, A. Ron, and N. Davidson, *Phys. Rev. Lett.* **100**, 223601 (2008).
- [5] P. K. Vudyasetu, R. M. Camacho, and J. C. Howell, *Phys. Rev. Lett.* **100**, 123903 (2008).
- [6] G. Heinze, A. Rudolf, F. Beil, and T. Halfmann, *Phys. Rev. A* **81**, 011401 (2010).
- [7] H. J. Coufal, D. Psaltis, and G. T. Sincerbox, *Holographic Data Storage*, 1st ed. (Springer, Berlin, Heidelberg, 2000).
- [8] I. Y. Dodin and N. J. Fisch, *Opt. Commun.* **214**, 83 (2002).
- [9] T. W. Mossberg, *Opt. Lett.* **7**, 77 (1982).
- [10] W. R. Babbitt and T. W. Mossberg, *Opt. Commun.* **65**, 185 (1988).
- [11] X. A. Shen and R. Kachru, *Opt. Lett.* **20**, 2508 (1995).
- [12] X. A. Shen, E. Chiang, and R. Kachru, *Opt. Lett.* **19**, 1246 (1994).
- [13] A. Y. Hamad and J. P. Wicksted, *Appl. Opt.* **40**, 1822 (2001).
- [14] M. Fleischhauer and M. D. Lukin, *Phys. Rev. A* **65**, 022314 (2002).
- [15] J. Ruggiero, J.-L. Le Gouët, C. Simon, and T. Chanelière, *Phys. Rev. A* **79**, 053851 (2009).
- [16] K. Surmacz, J. Nunn, K. Reim, K. C. Lee, V. O. Lorenz, B. Sussman, I. A. Walmsley, and D. Jaksch, *Phys. Rev. A* **78**, 033806 (2008).
- [17] Y. Tu, G. Zhang, Z. Zhai, and J. Xu, *Phys. Rev. A* **80**, 033816 (2009).
- [18] Z. Zhai, Y. Dou, J. Xu, and G. Zhang, *Phys. Rev. A* **83**, 043825 (2011).
- [19] Z. Zhai, Y. Tu, Y. Dou, J. Xu, and G. Zhang, *Opt. Commun.* **285**, 277 (2011).
- [20] M. Nilsson, L. Rippe, S. Kröll, R. Klieber, and D. Suter, *Phys. Rev. B* **70**, 214116 (2004).
- [21] B. S. Ham, M. S. Shahriar, M. K. Kim, and P. R. Hemmer, *Opt. Lett.* **22**, 1849 (1997).
- [22] R. W. Equall, R. L. Cone, and R. M. Macfarlane, *Phys. Rev. B* **52**, 3963 (1995).
- [23] F. Beil, J. Klein, G. Nikoghosyan, and T. Halfmann, *J. Phys. B* **41**, 074001 (2008).
- [24] A. V. Turukhin, V. S. Sudarshanam, M. S. Shahriar, J. A. Musser, B. S. Ham, and P. R. Hemmer, *Phys. Rev. Lett.* **88**, 023602 (2001).
- [25] A. L. Alexander, J. J. Longdell, M. J. Sellars, and N. B. Manson, *Phys. Rev. Lett.* **96**, 043602 (2006).
- [26] G. Hétet, J. J. Longdell, A. L. Alexander, P. K. Lam, and M. J. Sellars, *Phys. Rev. Lett.* **100**, 023601 (2008).
- [27] D. L. McAuslan, P. M. Ledingham, W. R. Naylor, S. E. Beavan, M. P. Hedges, M. J. Sellars, and J. J. Longdell, *Phys. Rev. A* **84**, 022309 (2011).
- [28] V. Damon, M. Bonarota, A. Louchet-Chauvet, T. Chanelière, and J.-L. Le Gouët, *New J. Phys.* **13**, 093031 (2011).